Cement and Concrete Composites 88 (2018) 73–85

Contents lists available at ScienceDirect

Cement and Concrete Composites

journal homepage: www.elsevier.com/locate/cemconcomp

An integrated design method of Engineered Geopolymer Composite

Motohiro Ohno, Victor C. Li*

Department of Civil and Environmental Engineering, University of Michigan, Ann Arbor, MI 48109-2125, United States

ARTICLE INFO

Article history:
Received 12 March 2017
Received in revised form
8 January 2018
Accepted 1 February 2018

Keywords:
Geopolymer
Fiber-reinforced composite
Design of experiment
Micromechanics
Material sustainability

ABSTRACT

Strain-hardening ductile fiber-reinforced geopolymer composite, named Engineered Geopolymer Composite (EGC), is a promising material for achieving green and durable civil infrastructure. Despite increasing attentions of the unique material, inefficient trial-and-error approaches are often employed in the material design, which slows the research and development. This paper proposed a new design methodology of EGC that integrates three design techniques: Design of Experiment (DOE), micromechanical modeling, and Material Sustainability Indices (MSI). The mix design of a preliminary version of EGC was optimized to achieve higher compressive strength, maintain high tensile ductility, and enhance the material greenness simultaneously. With the aid of the systematic design process, an optimized EGC with improved compressive strength of 43.1 MPa and high tensile ductility of 4.7% was developed, while achieving 11% less embodied energy and 55% less CO_2 equivalent emissions compared with a standard Engineered Cementitious Composite (ECC). Therefore, the applicability and effectiveness of the proposed design method were successfully demonstrated.

1. Introduction

Ductile fiber-reinforced geopolymer composites have been recently proposed for green and durable civil infrastructure [1]. In essence, the new material technology combines geopolymer [2–4] and Engineered Cementitious Composite (ECC) [5,6]. Enhanced material greenness is attributed to the geopolymer matrix; it relies on no ordinary portland cement (OPC) but can use industrial byproducts, such as fly ash and slag, for the primary ingredient. Low carbon footprints of cement-free geopolymer concrete have been estimated by many researchers [7–10]. Besides the high material greenness, fiber reinforcement imparts improved durability to the material, as reported in ECC materials [11–13]. Synergistic interaction between fiber and matrix offers the strain-hardening characteristic and high tensile ductility, suppressing inherent brittleness of the geopolymer matrix. Further, when the material is overloaded, damage is distributed as self-controlled multiple microcracks. The tight cracking enables the ductile geopolymer to maintain their mechanical and durability properties even when highly damaged. With these unique properties, a new family of ductile fiber-reinforced geopolymer composites – named Engineered Geopolymer Composite (EGC) – shows great promise as a sustainable construction material. So far, several previous studies have demonstrated the feasibility of ductile geopolymer composites and reported their strain-hardening behavior and multiple-cracking characteristics in tension and flexure [14–17].

While EGC is increasingly gaining attention in the research field, difficulty in the material design slows the research and development. One of the biggest challenges is the large number of design variables. Geopolymer matrix typically involves more design variables than cement matrix, including types of alkaline activators and solid aluminosilicate materials, their mix proportions, curing regimes, *etc.* Moreover, optimization of fiber and fiber/matrix interface properties is also required for EGC, which further expands the degrees of freedom in the material design. As a result, empirical trial-and-error approaches, which have been often employed in the research field, are inefficient to explore the vast design space.

It should be also noted that EGC design is a multi-response optimization problem. Many prior studies on geopolymer design are only focused on compressive strength. Typically, a series of specimens are prepared by varying several design factors (*e.g.* type of alkaline activator, activator/fly ash ratio, *etc.*), and an optimum design that provides the best response (*i.e.* compressive strength) is determined. This traditional approach, however, is ineffective for EGC development; high tensile ductility and enhanced material greenness are desired properties in EGC optimization, as well as fundamental mechanical properties such as compressive strength. Finding an optimum mix design to simultaneously improve those

* Corresponding author.
E-mail address: vcli@umich.edu (V.C. Li).

https://doi.org/10.1016/j.cemconcomp.2018.02.001
0958-9465/

multiple responses is time and cost intensive when relying on the conventional trial-and-error approach. To facilitate research and development of EGC materials, more efficient and systematic design methodologies are needed.

This paper proposes a new design methodology for strain-hardening fiber-reinforced geopolymer composites with high tensile ductility and multiple micro-cracking characteristics. The Design of Experiment (DOE), micromechanical modeling, and material sustainability indices (MSI) are integrated to simultaneously achieve higher strength, ductility, and material greenness. The concept and design process of the integrated design method are first outlined in the following section. Then, analytical and experimental investigations are conducted to demonstrate the applicability and effectiveness of the design method. Consequently, a green and ductile (and, therefore, durable) EGC material is systematically developed.

2. Integrated design method

Fig. 1 illustrates the design scheme of the proposed integrated method. It consists of three design phases: matrix, composite, and environmental designs, each of which utilizes a specific material design technique.

The matrix design phase is aimed at meeting requirements in fundamental engineering properties such as compressive strength. Design variables (types of ingredients, mix proportions, curing regime, *etc.*) are optimized to achieve required performances, with the aid of a statistics-based design method, called Design of Experiment (DOE). Specifically, the method used in this study was developed by Taguchi [18] and has been applied to numerous science and engineering fields. In this approach, effects of design variables (or "input factors") on performance (or "output") are systematically quantified without explicitly testing every combination of input factors. Out of a number of possible combinations of input variables, only a portion of them is selected to test, based on a fractional-factorial design planned by using an orthogonal array (OA). The test results are then investigated based on the Analysis of Variance (ANOVA) method. The detailed theories can be found in literature (e.g. Ref. [19]). With this technique, experimental costs can be substantially reduced, yet robust information about the relationship between design variables and properties of interest is obtained.

Once a desired matrix is developed, fiber and fiber/matrix interface properties are tailored to impart high tensile ductility and multiple-cracking characteristics to the material. The micromechanical modeling is a design technique adopted in the composite design phase [20]. For given matrix and fibers, micromechanical parameters (matrix fracture toughness, bonding properties between fiber and matrix, *etc.*) that govern the composite tensile properties are measured by experimental techniques. Then, the composite tensile behavior is simulated by using an analytical model based on fracture mechanics, micromechanics and probabilistic models. The simulation result guides required modification on micromechanical parameters for achieving desired tensile ductility and tight multiple cracking. With the aid of the micromechanical modeling, rapid development of various types of Engineered Cementitious Composites (ECCs), including lightweight, self-compacting, sprayable, and self-healing ECCs, has been realized.

The last phase is the environmental design that evaluates overall sustainability of the developed composite. In this study, the Material Sustainability Indices (MSI) are employed to measure the embodied energy consumption and carbon footprints associated with the material production [21]. MSI values represent a partial life cycle analysis (LCA) of the material greenness that accounts for raw material acquisition, processing, and manufacturing while the use and disposal phases are omitted. MSI are useful for quantifying the overall environmental performance of materials, regardless of

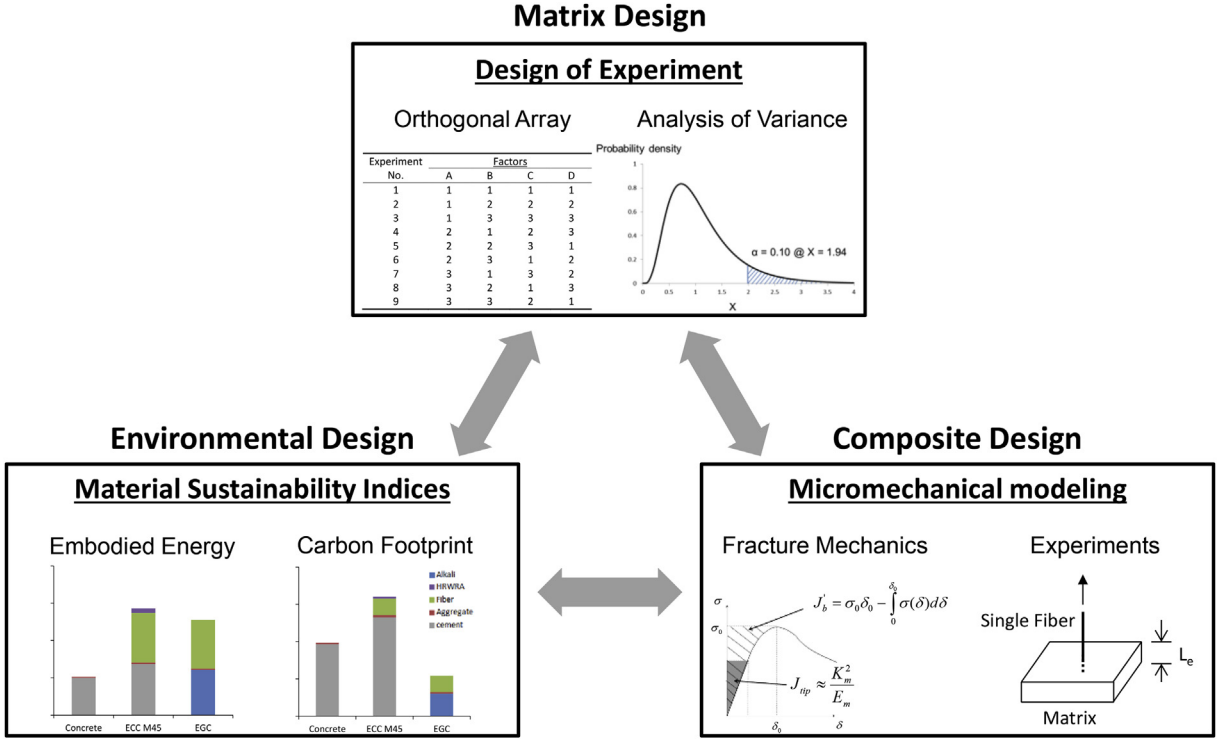

Fig. 1. Design scheme of the proposed integrated design method that combines three design techniques for matrix, composite, and sustainability design phases.

the application, and compare the carbon and energy footprints of different materials on a mass or volume basis.

Those three design stages are linked with each other and work in a synergistic manner. For example, sustainability aspects are considered in both the beginning matrix design stage and subsequent composite design stage by pre-screening out energy/carbon-intensive ingredients. In addition, design variables that are found to be "insignificant factors" based on the DOE study can be used to either modify micromechanical parameters in the composite design stage or lower the energy/carbon footprints for the environmental design. This integrated design scheme enables systematic optimization for multiple objectives that EGC materials sort to satisfy.

A preliminary version of EGC has been developed by the authors [15], which has high tensile ductility of over 4% but relatively low compressive strength of 27.6 MPa. In this study, the proposed integrated design method is used to (1) improve the compressive strength, (2) maintain the high tensile ductility, and (3) lower the energy and carbon footprints of the EGC simultaneously. The detailed design process adopted in this study is presented in the following section.

3. Matrix development

A DOE study is conducted to modify the mix design of the preliminary EGC matrix (shown in Table 1) for achieving higher compressive strength.

3.1. Materials and methods

Two types of fly ash were blended in the mixture, labeled Fly ash A and B, respectively, both of which were classified as class F fly ash as designated by ASTM C 618 [22]. Table 2 lists the chemical compositions and physical properties of the fly ashes reported from the manufacturer. F-75 Ottawa silica sand was used as aggregate. The alkaline activator was prepared by dissolving laboratory-grade sodium hydroxide (NaOH) pellets in mixture of sodium silicate solution (Na_2SiO_3 with 8.9 wt% Na_2O, 28.7 wt% SiO_2, and 62.5 wt% H_2O) and tap water (labeled "Pre-mix water" in Table 1). The solution preparation was done at least 24 h before its use as the activator for geopolymer so that chemical equilibrium was attained. Additional water (labeled "Mix water" in Table 1) was used when mixed with solid materials (i.e. fly ash and silica sand) to obtain adequate rheology.

The mix design of the preliminary EGC matrix was different from those of typical geopolymer mortars in two aspects. First, two types of fly ash were blended to control the hardening property of geopolymer mortar. When the fly ash A was singly used as the reactant, specimens did not stiffen enough and fractured in demolding one day after casting. On the other hand, the use of fly ash B by itself resulted in too fast setting time to cast in molds. These problems are likely to be related to the different amount of CaO content between Fly ash A and B. Second, tap water (Pre-mix water) was used to prepare the alkaline activator, while extra water (*i.e.* Mix water) was added during the mortar mixing. It was found during the development of the preliminary EGC that adding the mix water to the alkaline activator beforehand (*i.e.* no extra water was added during the mortar mixing) resulted in different viscosity and flowability of the fresh geopolymer mortar. The reason for this is unclear and further research will be required.

Table 1
Mix proportion of preliminary EGC matrix (by mass).

Fly ash A	Fly ash B	Sand	Na_2SiO_3	NaOH (pellet)	Pre-mix water	Mix water
0.8	0.2	0.3	0.256	0.056	0.039	0.12

Table 2
Chemical compositions and physical properties of fly ash.

	Fly ash A	Fly ash B
SiO_2	46.09	42.20
Al_2O_3	23.15	22.51
Fe_2O_3	19.48	9.20
CaO	5.08	15.66
SO_3	0.77	1.85
MgO	1.12	3.20
Na_2O	0.58	0.98
K_2O	1.73	1.53
Moisture	0.16	0.12
Loss on ignition	1.99	1.34
density	2.58	2.53
Fineness (% retained on 45 μm sieve)	22.24	16.58

For the mortar mixing, fly ash and silica sand were first dry-mixed for 2 min. The activator solution and mix water were then added to the mixture. After the fresh mortar reached the desired fresh state, the mixture was cast into molds on a vibration table and cured at a room temperature (23 ± 3 °C) for 24 h. Subsequently, the specimens were cured in an oven at 60 °C for 24 h, followed by air curing at a room temperature until the age of 28 days prior to testing. To measure the compressive strength, three 2-inch (51-mm) cube specimens were prepared for each mix proportion and subjected to uniaxial compression.

3.2. Statistical design approach

In this study, six ratios of the ingredients by mass were investigated as the design variables:

(1) $FA_{(B)}/FA$ – ratio of fly ash B to the total amount of fly ashes (i.e. fly ash A plus B)
(2) S/FA – ratio of silica sand to FA
(3) Alk/FA – alkaline activator to FA ratio where Alk is the total amount of Na_2SiO_3 solution, NaOH pellets, and pre-mix water
(4) $Na_2SiO_3/NaOH_{(sol)}$ – ratio of Na_2SO_3 to NaOH solution where $NaOH_{(sol)}$ is the total amount of NaOH pellets and pre-mix water
(5) Pre-W/$NaOH_{(sol)}$ – reflecting the concentration of NaOH solution where Pre-W is the amount of pre-mx water, and
(6) Mix-W/FA – ratio of mix water to FA, which affects the rheology of the mixture.

These design variables were determined so that the values could be simply calculated by taking the mass ratio of ingredients. Also, the pre-mix water and mix water were separately considered, based on the finding in the preliminary study mentioned in the preceding section. As a result, however, the design variables here are somewhat different from those commonly used in geopolymer design. For example, the definition of the alkaline activator in this study does not include the mix water, while many past studies defined the alkaline activator including the total amount of water used. Also, Na_2O content and Ms modulus (SiO_2/Na_2O molar ratio) of the alkaline activator are often used in the research community to reflect the availability of alkali ions or silica, but this study used $Na_2SiO_3/NaOH_{(sol)}$ and Pre-W/$NaOH_{(sol)}$ instead. Thus, in the following results and discussion section, those common parameters were also calculated for each mix proportion so that the test results

in this study could be compared with those in many prior studies.

In the preliminary EGC matrix, those six ratios were (1) 0.2, (2) 0.3, (3) 0.35, (4) 2.7, (5) 0.41, and (6) 0.12, respectively. To quantify individual effects of the six factors, three different factor levels were considered for each mixing ratio, meaning that there are $3^6 = 729$ possible combinations.

L18 orthogonal array was adopted in this study to assign the six factors with three levels each. The factor levels and corresponding absolute values of each mixing ratio are shown in Table 3. The L18 orthogonal array can accommodate 1 two-level factor and 7 three-level factors, testing only 18 combinations. In some types of orthogonal arrays and their arrangements, interaction effects between factors are confounded with a specific factor effect, leading to misevaluation on the main effect. The advantage in use of the L18 orthogonal array is that all the interaction effects are almost evenly spread across main factor effects, allowing more accurate evaluations on the main effects. When only 6 three-level factors are considered, they should be assigned to the third through eighth columns so that the degree of uniform distribution of confounding is maximized. Therefore, the first and second columns are set as empty columns that have no assigned factors. Based on the prepared L18 orthogonal array, three 2-inch (51-mm) cubes were cast for each of the 18 different mix proportions.

Using the resulting experimental data, an ANOVA study was conducted to analyze the relationship between each design variable and the output (*i.e.* compressive strength). The sum of squares (SS) for each factor, which reflects deviation from the mean caused by the factor, was calculated and then normalized by the degree of freedom (DOF) to find the mean square (MS). SS and MS for error were also computed to measure the variation attributed to inherent experimental errors. Subsequently, the F-ratio was calculated for each factor by taking the ratio of MS-for-factor to MS-for-error, the magnitude of which reflects the significance of the factor on the output. Finally, factors were classified as either significant or insignificant factors based on a statistical F-test with 5% significance level.

It should be mentioned that trends of factor effects in the above approach are derived from the selected ranges of the factor levels. It is possible that a different trend is found outside the ranges, resulting in a different conclusion on the significance of the factors. Nevertheless, a lot of insights on the main factor effects can be obtained from a minimal number of experiments, predicting the most promising direction for optimization of the design variables. In addition, confirmation experiments are typically conducted to verify the prediction from the analysis results. Based on those findings, an optimum mix proportion of EGC matrix can be determined by selecting optimum levels for significant factors.

3.3. Results and discussion

Table 4 lists compressive strength of the 18 mixtures with three specimens each. The SS, MS, and F-ratio of each factor are summarized in Table 5. According to the ANOVA results, the most influential factor is Pre-W/$NaOH_{(sol)}$, which reflects the concentration of NaOH solution. The second highest F-ratio is found in Mix-W/FA, which affects the rheology of the mixture and is therefore assumed to affect the pore size distribution of the hardened matrix. The third most significant factor is $FA_{(B)}$/FA, followed by S/FA. The other factors – Alk/FA and $Na_2SiO_3/NaOH_{(sol)}$ – are suggested to be insignificant within the selected ranges of the factor levels since those F-ratios are less than the theoretical F-score at 5% significance level (i.e. $F_{0.05,2,41} = 3.23$).

To investigate trends of the factor effects, main-effects plots that plot mean compressive strength at each level of parameters are

Table 4
Compressive strength of 18 EGC mixtures with 3 samples each (in MPa).

Mix no.	Measured compressive strength (3 samples)			Mean	Standard deviation
1	45.5	33.9	31.5	37.0	7.5
2	33.5	33.1	33.0	33.2	0.3
3	24.9	27.4	26.2	26.2	1.3
4	24.3	21.8	22.1	22.7	1.3
5	50.1	49.7	53.1	51.0	1.8
6	49.2	48.6	49.0	48.9	0.3
7	26.9	26.7	28.3	27.3	0.9
8	39.3	37.6	37.0	38.0	1.2
9	40.5	38.7	43.4	40.8	2.4
10	38.0	34.5	39.5	37.4	2.6
11	27.6	31.1	32.1	30.3	2.3
12	52.7	39.9	35.6	42.7	8.9
13	32.6	38.5	36.5	35.9	3.0
14	46.8	46.8	47.9	47.2	0.6
15	44.6	45.4	45.5	45.2	0.5
16	47.0	43.0	43.7	44.6	2.1
17	34.1	33.8	37.4	35.1	2.0
18	38.9	36.0	37.1	37.3	1.5

Table 3
L18 orthogonal array for EGC matrix development.

Mix no.	Assigned factors, their absolute values and codes (levels)							
	_	–	$FA_{(B)}$/FA	S/FA	Alk/FA	$Na_2SiO_3/NaOH_{(sol)}$	Pre-W/$NaOH_{(sol)}$	Mix-W/FA
1	(1)	(1)	0.2 (1)	0.2 (1)	0.30 (1)	2.4 (1)	0.31 (1)	0.10 (1)
2	(1)	(1)	0.3 (2)	0.3 (2)	0.35 (2)	2.7 (2)	0.41 (2)	0.12 (2)
3	(1)	(1)	0.4 (3)	0.4 (3)	0.40 (3)	3.0 (3)	0.51 (3)	0.14 (3)
4	(1)	(2)	0.2 (1)	0.2 (1)	0.35 (2)	2.7 (2)	0.51 (3)	0.14 (3)
5	(1)	(2)	0.3 (2)	0.3 (2)	0.40 (3)	3.0 (3)	0.31 (1)	0.10 (1)
6	(1)	(2)	0.4 (3)	0.4 (3)	0.30 (1)	2.4 (1)	0.41 (2)	0.12 (2)
7	(1)	(3)	0.2 (1)	0.3 (2)	0.30 (1)	3.0 (3)	0.41 (2)	0.14 (3)
8	(1)	(3)	0.3 (2)	0.4 (3)	0.35 (2)	2.4 (1)	0.51 (3)	0.10 (1)
9	(1)	(3)	0.4 (3)	0.2 (1)	0.40 (3)	2.7 (2)	0.31 (1)	0.12 (2)
10	(2)	(1)	0.2 (1)	0.4 (3)	0.40 (3)	2.7 (2)	0.41 (2)	0.10 (1)
11	(2)	(1)	0.3 (2)	0.2 (1)	0.30 (1)	3.0 (3)	0.51 (3)	0.12 (2)
12	(2)	(1)	0.4 (3)	0.3 (2)	0.35 (2)	2.4 (1)	0.31 (1)	0.14 (3)
13	(2)	(2)	0.2 (1)	0.3 (2)	0.40 (3)	2.4 (1)	0.51 (3)	0.12 (2)
14	(2)	(2)	0.3 (2)	0.4 (3)	0.30 (1)	2.7 (2)	0.31 (1)	0.14 (3)
15	(2)	(2)	0.4 (3)	0.2 (1)	0.35 (2)	3.0 (3)	0.41 (2)	0.10 (1)
16	(2)	(3)	0.2 (1)	0.4 (3)	0.35 (2)	3.0 (3)	0.31 (1)	0.12 (2)
17	(2)	(3)	0.3 (2)	0.2 (1)	0.40 (3)	2.4 (1)	0.41 (2)	0.14 (3)
18	(2)	(3)	0.4 (3)	0.3 (2)	0.30 (1)	2.7 (2)	0.51 (3)	0.10 (1)

Table 5
ANOVA results on six design variables of EGC matrix (unpooled).

Factors	DOF	Sum of square	Mean square	F-ratio
$FA_{(B)}$/FA	2	377	189	7.47
S/FA	2	242	121	4.80
Alk/FA	2	0.903	0.452	0.0179
$Na_2SiO_3/NaOH_{(sol)}$	2	92.9	46.4	1.84
Pre-W/$NaOH_{(sol)}$	2	1330	665	26.3
Mix-W/FA	2	530	265	10.5
Error	41	1035	25.2	–
Total	53	3608	–	–

Note: $F_{0.01,2,41} = 5.16$, $F_{0.05,2,41} = 3.23$, $F_{0.10,2,41} = 2.44$.

prepared for the test results (Fig. 2). As can be seen, an increase of Pre-W/$NaOH_{(sol)}$ and Mix-W/FA monotonically lowers the compressive strength in the selected ranges. In contrast, an increase of $FA_{(B)}$/FA and S/FA raises the compressive strength. Besides, statistically insignificant effects of Alk/FA and $Na_2SiO_3/NaOH_{(sol)}$, as mentioned above, can be seen in the plots.

Some of those observed trends agree with previous studies while the others do not. Regarding either Pre-W/$NaOH_{(sol)}$ or Mix-W/FA ratio, it is consistent with research findings by Hardjito and Rangan [23] that a higher amount of water in the mixture reduces the compressive strength. The observed trend of $FA_{(B)}$/FA is also in agreement with reported effects of calcium compounds on the compressive strength of geopolymer materials [24]. Since fly ash B contains a larger amount of calcium oxide (CaO) than fly ash A, it is suggested that a higher $FA_{(B)}$/FA ratio would cause more formation of C-S-H gel in the geopolymer matrix, contributing to higher compressive strength development, as reported by Yip et al. [25]. On the other hand, the fact that compressive strength increases with an increase of S/FA ratio does not agree with a previous study by Thakur and Ghosh [26]. The insignificant effects of Alk/FA and $Na_2SiO_3/NaOH_{(sol)}$ seem inconsistent with the study by Hardjito and Rangan [23] and many other studies.

However, as mentioned in the preceding section, the factors used in this study are somewhat different from commonly used parameters in past studies, and therefore direct comparison with previous findings may be misleading. For doing a fair comparison, four commonly used parameters are calculated for 54 samples (*i.e.* 3 specimens for 18 mixtures) and plotted with their compressive strength (Fig. 3).

Regarding the relationship between compressive strength and the ratio of the alkaline activator to FA, no significant correlation can be seen as the data are largely scattered in the selected range. Thus, it seems difficult to find an optimum mix design of the geopolymer matrix based on this parameter. In contrast to the finding here, the alkaline activator-to-FA ratio is often considered an influential factor on strength of geopolymer materials and has been intensively studied in the research field.

As an alternative design parameter, Hardjito and Rangan [23] proposed "water-to-geopolymer solids ratio" based on their extensive experimental investigation on effects of various design parameters on compressive strength and workability of fly ash-based geopolymer concrete. The water-to-geopolymer solids ratio represents the ratio of the total mass of water (including water contained in Na_2SiO_3 and NaOH solution) to the total mass of fly ash and solids in Na_2SiO_3 and NaOH solution. In the present case, both the pre-mix water and mix water are included in the total amount of water. Hardjito and Rangan found that the compressive strength of geopolymer concrete decreases as the ratio of water-to-geopolymer solids ratio increases [23].

In the obtained results in this study, a general decreasing trend can be seen for the water-to-geopolymer solids ratio, compared to

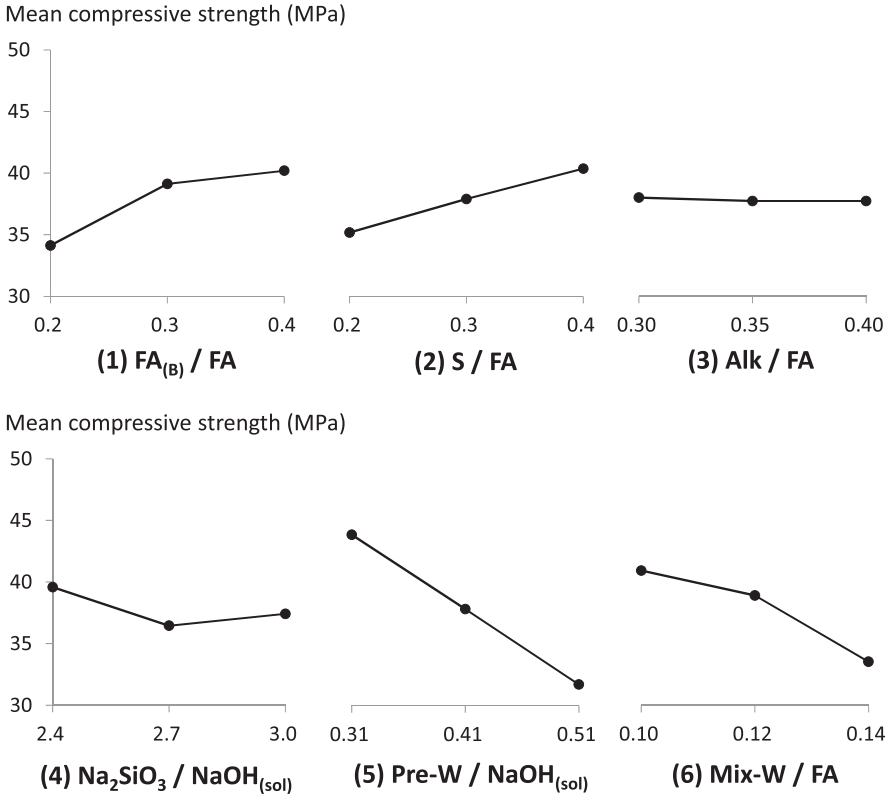

Fig. 2. Mean responses at each level of factors are plotted to visualize the main factor effects.

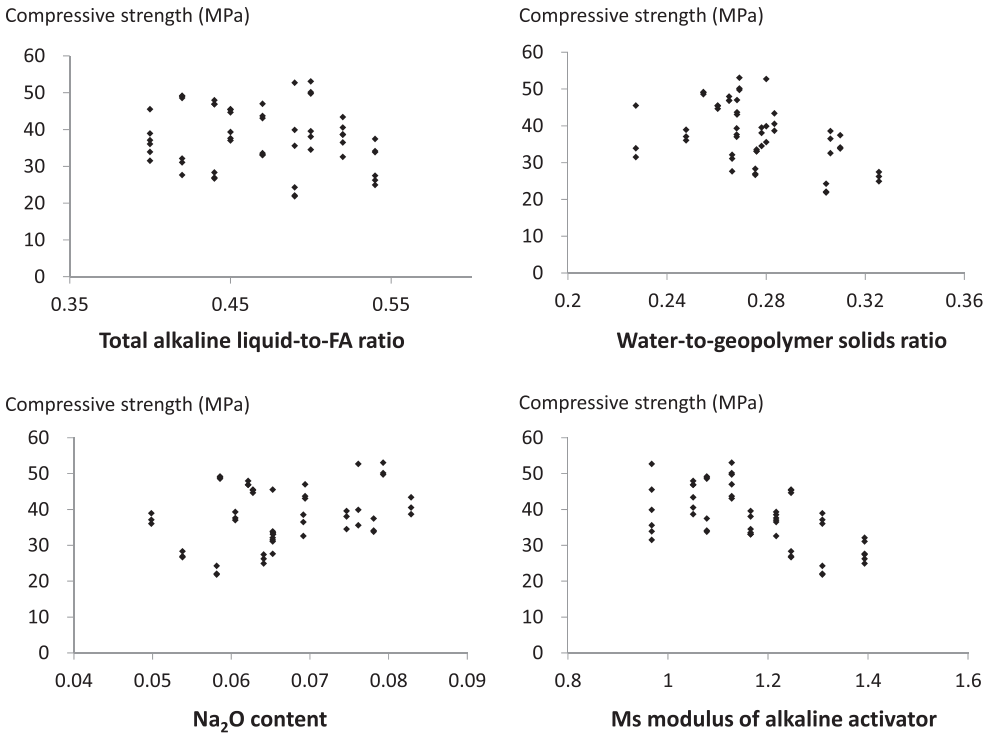

Fig. 3. Plots of compressive strength versus four parameters commonly used in past research, for 54 samples tested in this study.

that for the alkaline activator-to-FA ratio (Fig. 3). However, large variations can be still seen in the data, especially for the ratio of around 0.27. This implies that a lower ratio does not always provide higher compressive strength.

In the case of the Na_2O content and Ms modulus of the alkaline activator, the observed trends somewhat agree with the findings from previous studies. The former parameter represents the mass ratio of Na_2O content in the alkaline activator to FA, and the latter indicates the molar ratio of SiO_2 to Na_2O in the activator. For the Na_2O content, previous studies reported general increasing trends in compressive strength (e.g. Refs. [27–30]), while the obtained data in the present study show a weak increasing trend (Fig. 3). On the other hand, a decreasing trend can be seen for the Ms modulus in this study, which is in agreement with findings in Refs. [27,31]. Nevertheless, relatively large variations in the data, especially for the plot of Na_2O content, should be noted.

The obtained results and above discussion imply the complex chemistry in geopolymer formation that has not been fully understood yet. While some parameters proposed in past studies seem to have a significant correlation with compressive strength, the observed large variations suggest that optimizing the geopolymer mix design based on general trends for those parameters are not straightforward. This would be a primary reason that there is currently no comprehensive design procedure for geopolymer concrete and that trial-and-error approaches are still often used in the research field.

For obtained results in the present study, a further study would be required to fully understand the mechanisms behind the relationships between those design variables and compressive strength of EGC mortar. Nevertheless, with the aid of the statistical approach, an optimum EGC mixture design can be systematically predicted, even without such complete understanding of the mechanisms.

3.4. Optimum conditions

According to the ANOVA results and the main-effects plots, optimum conditions for the significant factors are (1) $FA_{(B)}/FA = 0.4$, (2) $S/FA = 0.4$, (5) $Pre\text{-}W/NaOH_{(sol)} = 0.31$, and (6) $Mix\text{-}W/FA = 0.10$. Due to their monotonic increasing/decreasing trend, it may be argued that a higher/lower ratio than the selected ranges could lead to further improvement on the compressive strength. However, it was found in a verification experiment that any of those directions resulted in too fast setting or too high viscosity of the fresh mixture to cast.

Meanwhile, due to their insignificant effects, factor levels of (3) Alk/FA and (4) $Na_2SiO_3/NaOH_{(sol)}$ can be set to any value in the selected ranges, without compromising the compressive strength. In the proposed integrated design scheme, these insignificant factors are utilized to complement optimization in the other design stages. For example, levels of those insignificant factors can be selected so that desired modifications on micromechanical parameters are made in the composite design phase. Besides, a higher material greenness can be achieved by choosing appropriate levels of those factors for the environmental design stage. In the present study, priority is put in the sustainability aspect. In the case of Alk/FA, it is obvious that a lower ratio of the factor provides a higher material greenness as fly ash is an industrial byproduct while the alkaline activator consists of primary products. On the other hand, a higher ratio is preferred for $Na_2SiO_3/NaOH_{(sol)}$ since Na_2SiO_3 production is less energy and carbon intensive than NaOH (detailed in Section 5). Therefore, (3) $Alk/FA = 0.3$ and (4) $Na_2SiO_3/NaOH_{(sol)} = 3.0$ were chosen for their optimum EGC matrix mixture. The resultant mixture design is presented in Table 6. The water-to-geopolymer solids ratio, alkaline activator-to-FA ratio, Na_2O content, and Ms modulus of the activator for this mix design are 0.23, 0.4, 0.059, and 1.1, respectively.

Table 6
Mix proportion of optimum EGC matrix (by mass).

Fly ash A	Fly ash B	Sand	Na_2SiO_3	NaOH (pellet)	Pre-mix water	Mix water
0.6	0.4	0.4	0.225	0.052	0.023	0.10

3.5. Verification experiment for compressive strength

To verify that the mix proportion predicted by the DOE study is indeed an optimum, verification experiments were conducted. Three 2-inch (51-mm) cube specimens of the predicted optimum EGC mortar were prepared and their compressive strength was measured as in the L18 experiments. Then, the measured compressive strength was compared with a statistically predicted mean and its confidence interval (CI). If the mean compressive strength of the confirmation experiment is inside the CI, then it is concluded that the predicted optimum condition is valid. Otherwise, more rounds of experiments will be required to detect any significant confounded interaction or unknown factor that was not taken into account in the first trial. The detailed procedures can be found in literature [19].

To calculate the predicted mean and its CI, SS and DOF of insignificant factors are combined with those of errors, which is a procedure known as 'pooling'. The pooled ANOVA results are summarized in Table 7. For the sake of brevity, columns of the L18 orthogonal arrays are labeled A through H from the left; the four significant factors – $FA_{(B)}$/FA, S/FA, Pre-W/$NaOH_{(sol)}$, and Mix-W/FA are therefore C, D, G, and H, respectively. Then, the predicated mean compressive strength of the optimum EGC mortar is expressed as:

$$\mu_{C_3D_3G_1H_1} = \overline{C}_3 + \overline{D}_3 + \overline{G}_1 + \overline{H}_1 - 3\overline{T} \tag{1}$$

where $\mu_{C_3D_3G_1H_1}$ is the predicted mean at the optimum condition, $\overline{X}_i$ represents the mean at i-th level of the parameter X (as plotted in the main-effects plots) and $\overline{T}$ is the total mean of all the data. The corresponding CI is given by the following equation:

$$CI = \sqrt{F_{\alpha;1;\nu_e} V_{ep}\left[\frac{1}{\eta_{eff}} + \frac{1}{r}\right]} \tag{2}$$

$F_{\alpha;1;\nu_e}$ represents the F-ratio at a significance level of α with the DOF of pooled errors ν_e; V_{ep} is the variance (equivalent to MS) of the pooled errors; η_{eff} is the effective number of replications expressed as (Total number of samples)/(1 + Total DOF associated with significant factors); r is the sample size for the confirmation experiment. In the present case, α, ν_e, V_{ep}, η_{eff} and r are 0.05, 45, 25.1, 6, and 3, respectively.

Table 8 presents the measured and predicted compressive strength of the optimum EGC matrix. As can be seen, the measured compressive strength of 50.5 MPa is quite close to the predicted mean of 52.0 MPa and inside the CI ranging from 44.8 to 59.1 MPa.

Table 7
Pooled ANOVA results on six design variables of EGC matrix.

Factors	DOF	Sum of square	Mean square	F-ratio
$FA_{(B)}$/FA	2	377	189	7.52
S/FA	2	242	121	4.83
Pre-W/$NaOH_{(sol)}$	2	1330	665	26.5
Mix-W/FA	2	530	265	10.6
Error	45	1129	25.1	–
Total	53	3608	–	–

Therefore, the result verifies the predicted optimum condition for EGC matrix mixture. Since the resultant compressive strength of 50.5 MPa is sufficiently high for various kinds of infrastructure applications, the primary objective of this matrix development stage was successfully achieved.

4. Composite design

In this design stage, the micromechanical modeling technique is used to develop a strain-hardening ductile EGC based on the optimized EGC matrix.

4.1. Micromechanical modeling

Tensile strain-hardening behavior of fiber-reinforced brittle mortar composites is realized by sequential formation of matrix micro-cracking. A fundamental requirement for the multiple cracking is steady-state flat crack propagation prevailing under tension. To ensure the steady-state cracking in composites reinforced with randomly oriented short fibers, the following strength- and energy-based criteria need to be met [32] [33]:

$$\sigma_{fc} \le \sigma_0 \tag{3}$$

$$J_{tip} \le \sigma_0\delta_0 - \int_0^{\sigma_0} \sigma(\delta)d\delta \equiv J_b' \tag{4}$$

The first condition requires that the first cracking strength (σ_{fc}) is lower than the fiber bridging capacity (σ_0) of the composite. σ_{fc} is determined by the flaw size and fracture toughness of the matrix while σ_0 depends on fiber and fiber/matrix interface properties. Violation of this criterion results in a single, localized crack formation with limited ductility. On the other hand, the second condition determines the crack propagation mode of the composite. J_{tip} is the crack tip toughness which represents the energy required for crack propagation. When the fiber content is small, J_{tip} approaches K_m^2/E_m where K_m and E_m are the fracture toughness and Young's modulus of the matrix. To achieve the flat crack propagation, J_{tip} should be lower than the complementary energy J_b' which is calculated from the fiber bridging stress σ versus crack opening δ relation (σ–δ relation) as shown in Fig. 4. Violation of this condition causes oval-shaped Griffith cracking [34]. When both the two conditions are satisfied, a flat crack initiates from a pre-existing flaw and extends indefinitely through the matrix. Repeated formation of such steady-state cracks lead to self-controlled multiple cracking and strain-hardening along with high ductility.

To ensure the satisfaction of the two criteria, determination of the crack bridging behavior is essential. Since the σ–δ relation is a result of synergistic interactions between fiber, matrix, and their interface, micromechanical parameters that govern the interactions need to be measured. A single-fiber pullout test, developed by Katzs and Li [35], is typically used to determine fiber/matrix interface properties including the frictional bond (τ_0), chemical bond (G_d), and slip hardening coefficient (β) [36]. Those measured micromechanical parameters are used to predict the composite behavior by using a scale-linking model [37]. The analytical scale-linking model accounts for the single-fiber bridging behavior and probabilistic distributions of orientations and embedment lengths of the numerous bridging fibers. σ_{fc}, σ_0, J_{tip}, and J_b' are determined based on the measured micromechanical parameters and the simulated σ–δ relation, and required modifications on the parameters, if needed, are systematically predicted for achieving desired composite tensile properties.

Table 8
Measured and predicted compressive strength of optimum EGC matrix (in MPa).

Measured compressive strength (3 samples)			Measured mean	Predicted mean	Predicted CI
50.2	50.9	50.5	50.5	52.0	[44.8, 59.1]

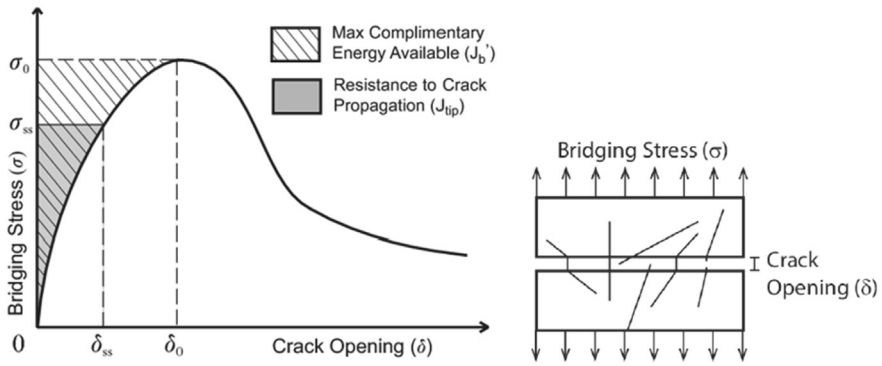

Fig. 4. Conceptual fiber bridging stress versus crack opening relation [61].

4.2. Experimental and analytical methods

For the optimized EGC matrix, small prismatic specimens with a single fiber embedded in the center were prepared for conducting the single-fiber pullout test. The specimen thickness (i.e. fiber embedment length) varied from 0.9 mm to 2.7 mm. Due to the preceding successful applications in ECC materials, polyvinyl alcohol (PVA) fiber with 1.2% oil coating by weight [38] was employed. From the obtained single-fiber pullout curves, τ_0, G_d, and β were computed based on the equations in Ref. [36]. To determine the matrix fracture toughness (K_m), notched beam specimens with 305 mm in length, 76 mm in height and 38 mm in thickness were prepared for conducting a three-point bending test. Four specimens with the notch depth-to-height ratio of 0.4 were tested in accordance with ASTM E399 [39]. In addition, four dogbone-shaped mortar specimens for uniaxial tension testing were prepared to measure the matrix Young's modulus (E_m) and the matrix tensile strength which was approximated as the composite first cracking strength (σ_{fc}). The rectangular gage section measured 100 mm in length, 30 mm in width, and 13 mm in thickness. All the specimens were subjected to the same curing condition as that in the DOE study and tested at the age of 28 days. The detailed testing configurations can be found in Refs. [40] and [41].

The σ–δ relation was computed by using a modified fiber-bridging constitutive law developed by Yang et al. [42]. For the sake of brevity, two-dimensional fiber distribution was assumed and both the matrix micro-spalling and the Cook-Gordon effect were not taken into account. The apparent strength [43], snubbing coefficient [43] and strength reduction factor [44] [45] of the PVA fiber were assumed to be the same as those found or estimated for cement matrix. To determine the effect of fiber volume fractions (V_f), three different input values of 1.0, 1.5, and 2.0% were used. The micromechanical parameters used in the simulation are listed in Table 9. From the predicted σ–δ relation, σ_0 and J_b' were determined to compare with experimentally measured σ_{fc} and J_{tip}.

4.3. Results and analysis

Table 10 summarizes the test results of the single-fiber pullout test, matrix fracture toughness test, and mortar-dogbone uniaxial tension test. The average chemical bond (G_d) between the optimized EGC matrix and PVA fiber is 6.1 J/m^2, which is 4–5 times higher than those found in ECC materials [38] [42]. On the other hand, the average frictional bond (τ_0) of 0.7 MPa and the average slip-hardening coefficient (β) of 0.33 for EGC are lower than those for ECC; Li and Wu reported 1.11 MPa and 1.15 for τ_0 and β, respectively [38], while Yang et al. found 1.31–1.91 MPa and 0.58–0.63 [42]. Thus, interfacial properties of EGC are significantly different from those of ECC materials. The reason for this is unclear, but it might be possible that interfacial layers between EGC matrix and PVA fiber consist of different types of compounds from those in PVA-ECC. A further research is required to investigate the microstructure and chemical compositions of EGC interfacial layers.

It should be also noted that the measured interfacial properties have large standard deviations. While such large variations have been often observed for the single-fiber pullout test in past studies (e.g. Ref. [36]), a verification experiment is important to verify the composite tensile behavior that was predicted based on the measured micromechanical parameters. This is presented in the following section.

Despite the large standard deviations, the average data of measured interfacial properties seem to represent general bonding characteristics of EGC matrix and PVA fiber. The strong chemical bond typically results in smaller crack width by limiting the crack opening during the strain-hardening stage. While the weaker frictional bond and smaller slip-hardening coefficient might cause lower bridging capacity (σ_0), a high tensile ductility can be achieved by suppressing fiber rupture and facilitating fiber pullout. Indeed, the preliminary version of EGC exhibited smaller average crack width than ECC materials, with high tensile ductility of over 4.5% [15].

Regarding the matrix properties, EGC matrix shows relatively weaker and more brittle characteristics than ECC matrix; the fracture toughness (K_m) of 0.37 MPa*m$^{1/2}$, Young's modulus (E_m) of 7.9 GPa, and tensile strength (approximated as σ_{fc}) of 1.4 MPa on average are about half of those of ECC materials [46] [47]. It should be mentioned, however, that this is beneficial for satisfying the strength- and energy-based criteria, as σ_{fc} and J_{tip} in Eqs. (3) and (4) are reduced. From these results, $J_{tip} \approx K_m^2/E_m$ was determined to be 17.3 J/m^2.

Fig. 5 shows the computed fiber bridging capacity (σ_0) and complementary energy (J_b') versus fiber volume fractions (V_f). As

Table 9
Micromechanical parameters used as model input.

Fiber properties					Interface properties	
Diameter (μm)	Length (mm)	Young's modulus (GPa)	Apparent strength (MPa)	Volume (%)	Snubbing coefficient	Strength reduction coefficient
39	12	42.8	1092[a]	1.0, 1.5, 2.0	0.2[b]	0.33[b]

[a] Reduced fiber strength when the fiber is embedded in cementitious matrix [38].
[b] Assumed values based on experiment [42].

Table 10
Measured micromechanical parameters of optimum EGC matrix.

Interface properties [a]			Matrix properties		
Chemical bond (J/m^2)	Frictional bond (MPa)	Slip-hardening coefficient	Fracture toughness ($MPa*m^{1/2}$)	Young's modulus (GPa)	Tensile strength (MPa)
6.1 ± 6.8	0.70 ± 0.38	0.33 ± 0.31	0.37 ± 0.02	7.9 ± 2.1	1.4 ± 0.4

[a] Averaged values of 42 specimens for single-fiber pullout test.

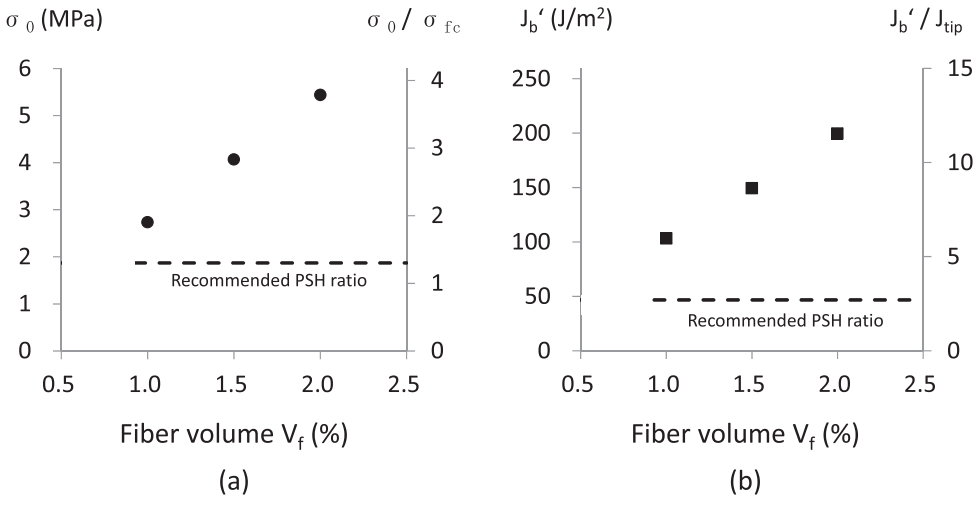

Fig. 5. Computed (a) fiber bridging capacity and (b) complementary energy with their PSH indices. Dashed lines indicate recommended PSH values for practical design [48].

can be seen, an increase of V_f elevates both σ_0 and J_b' almost linearly. It is obvious that the fiber content has a significant impact on tensile properties of the composite. In addition, the ratios of σ_0/σ_{fc} and J_b'/J_{tip} – called pseudo strain-hardening (PSH) index for strength and energy, respectively – are shown in the graphs of Fig. 5. Both of them are greater than unity for all the series, meaning that both the strength- and energy-based criteria are satisfied. According to the analytical and experimental study by Kanda and Li [48], $\sigma_0/\sigma_{fc} \geq 1.3$ and $J_b'/J_{tip} \geq 2.7$ are recommended to achieve robust tensile strain-hardening in ECC, due to the material variability caused by the random matrix flaw size and fiber dispersion. The computed energy PSH values are considerably higher than the recommended value, while there is a smaller margin between the computed strength PSH index of the V_f-1.0% case and the recommended value. If any of the computed PSH values violates either of the two necessarily conditions, appropriate modifications will be done on the micromechanical parameters, including a different length, diameter, volume fraction, or oiling quantity [38] of the PVA fiber. Use of a different type of fiber, such as polyethylene (PE) or polypropylene (PP) fiber, is another possibility. In this study, the predicted $\sigma-\delta$ relation suggests that the optimized EGC matrix reinforced with the PVA fiber can exhibit tensile strain-hardening and multiple cracking with high ductility, even for a fiber volume fraction of 1.0%.

4.4. Verification experiment for tensile ductility

To verify the prediction by the micromechanical modeling study, a verification experiment was conducted. Particularly, the test aimed to confirm if the EGC with 1.0% fiber volume could exhibit significant strain-hardening behavior with high tensile ductility of over 3% (i.e. comparable performance to ECC materials). Three batches of the optimized fresh EGC mortar were prepared and PVA fiber was slowly added so that each of the batches had the fiber content of 1.0, 1.5, and 2.0%. Four dogbone-shaped specimens were prepared from each of the mixture and subjected to the same curing condition as that in the DOE study. In addition, three 2-inch (51-mm) cube specimens were prepared to measure the composite compressive strength. Uniaxial compressive and tensile tests were conducted at the specimen age of 28 days.

Fig. 6 shows the tensile stress-strain curves of the EGC specimens with three different fiber volume fractions. As predicted, all the series exhibit strain-hardening behavior with high tensile ductility. However, EGC with 1% fiber volume shows relatively large load drops during the strain-hardening stage, which is associated with the larger crack width than the other cases. Moreover, variability among specimens is large and both the first cracking strength (σ_{fc}) and ultimate tensile strength (i.e. fiber bridging capacity σ_0) are also limited.

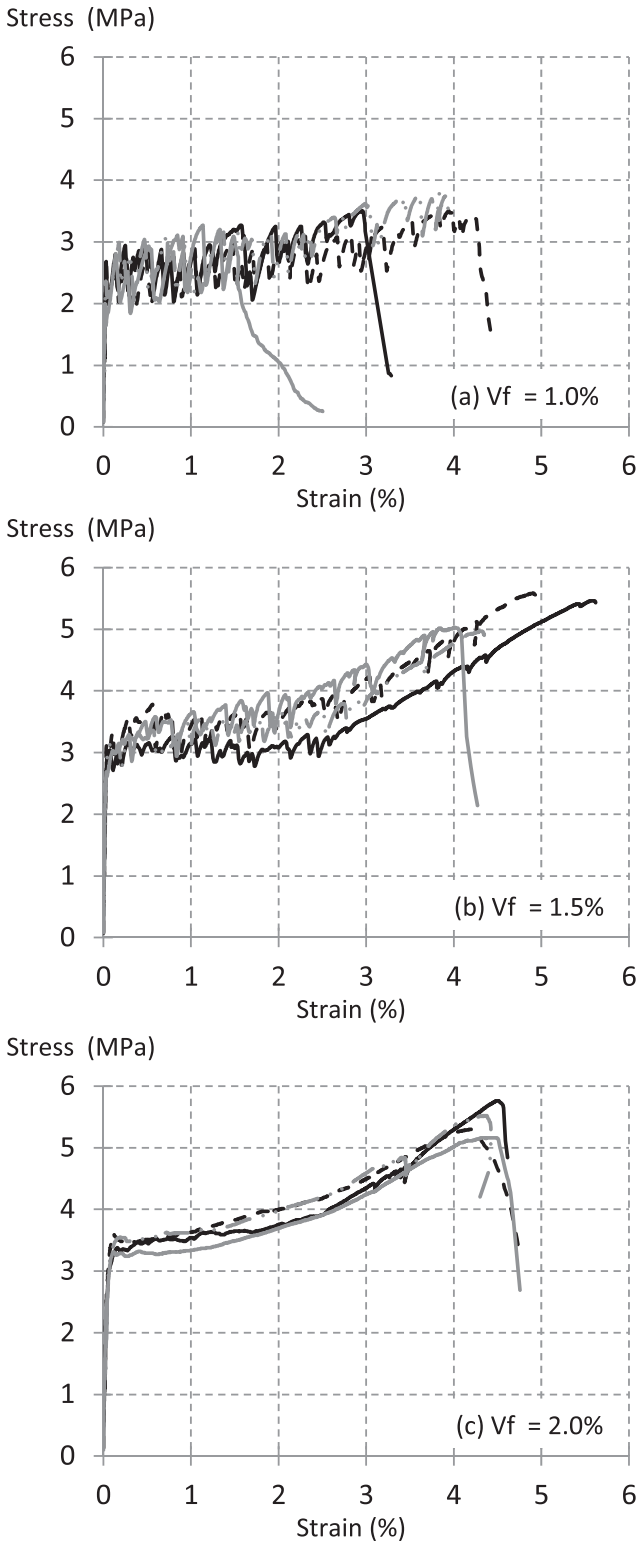

Fig. 6. Tensile stress-strain curves of all EGC series show strain hardening with high ductility.

The degree of the variability is clearly related to the predicted PSH indices. While both the strength and energy PSH indices are greater than the recommended values, the margin gets smaller as the fiber volume is decreased, as shown in Fig. 5. Variability among specimens, especially in tensile ductility, gets larger with the reduced fiber content. Therefore, PSH indices determine the degree of robustness of tensile ductility, as well as the satisfaction of the strength and energy criteria.

Table 11 summarizes the measured mechanical properties of the three series of EGC. As the fiber volume increases, the compressive strength, first cracking strength and ultimate tensile strength are all increased. While the composite compressive strength is unexpectedly lower than the EGC mortar, EGC with 1.5% and 2.0% fiber volume fractions have adequate strength of over 40 MPa, which is appropriate for various applications. The ductility of EGC with 1.5% V_f is slightly larger than EGC with 2.0% V_f, but the variability among specimens is much smaller in the 2.0% case.

Interestingly, the observed strength PSH indices in Table 11 (i.e. ratio of the ultimate composite tensile strength to the first cracking strength observed in the experiment) are considerably lower than the model predicted values. This discrepancy results from the difference between the observed first cracking strength and the mortar tensile strength that was used as the model input. As can be seen in Fig. 6, the composite first cracking strength is higher than the mortar strength of 1.4 MPa and increases with an increment of the fiber volume, while the same value was used for all the three cases in the model. The composite first cracking strength was determined by a point of the stress-strain curve after which a significant non-linearity was observed. However, Yang and Li showed in their numerical simulation study [49] that, when the matrix tensile strength is low compared with cohesive traction associated with fiber bridging, composite stress at the peak, after which a significant non-linearity occurs (and the steady-state cracking stage begins), can be larger than the matrix strength due to the enhanced role of the fiber bridging. Due to the higher first cracking strength of the composite, the observed strength PSH values reported in Table 11 can apparently be lower than the model predicted values.

While all the EGC series have strain-hardening and multiple-cracking characteristics with high tensile ductility, it was found that smaller fiber content lowers compressive and tensile strength and causes larger variability in the ductility. Due to the adequate compressive strength and excellent tensile properties, EGC with 1.5 and 2.0% V_f are promising for large-scale infrastructure applications. In the following section, material greenness of these two series is examined in the final environmental design stage.

5. Environmental performance comparison

5.1. Materials and methods

Environmental performances of the developed EGC-1.5% and EGC-2.0% were compared with that of the preliminary version of EGC, in terms of the Material Sustainability Indices (MSI) [21]. For references, MSI of normal cement concrete and ECC materials were also investigated. In the present study, embodied energy consumption and global warming intensity (GWI) associated with unit volume of the materials were calculated by accounting for all the required energy and generated emissions in the cradle-to-gate phases: raw material acquisition, processing and manufacturing. For the carbon footprints calculation, 100-year global warming potential (GWP) values of the ICPP 2013 report [50] were used to calculate the carbon dioxide (CO_2) equivalent emissions.

Life cycle inventory data of the ingredients used in this study are listed in Table 12. The data were collected from scientific literatures and environmental reports from industrial bodies, which report both the energy consumption and greenhouse gas emissions and have significance in the research field. The carbon intensity associated with temperature curing of EGC was obtained from a study

Table 11
Mechanical properties of EGC with three different fiber volume fractions.

Series	Compressive strength (MPa)	Tensile strain capacity (%)	First cracking strength (MPa)	Ultimate tensile strength (MPa)	Strength PSH
V_f–1.0%	38.5 ± 5.4	3.0 ± 1.3	2.5 ± 0.3	3.5 ± 0.2	1.40
V_f–1.5%	43.1 ± 3.0	4.7 ± 0.7	2.9 ± 0.2	5.3 ± 0.3	1.83
V_f–2.0%	43.3 ± 1.0	4.4 ± 0.1	3.5 ± 0.1	5.4 ± 0.3	1.54

Table 12
Life cycle inventories of raw ingredients of concrete, ECC and EGC materials.

Ingredients	Embodied energy (MJ/kg)	GWI (kg CO_2-eq/kg)
Portland cement [59]	4.8	0.93
Coarse/fine aggregate [60]	0.12	0.0062
Fine silica sand [61]	0.17	0.025
Fly ash [60]	0.11	0.0074
PVA fiber [62]	101	3.4
Super plasticizer [61] [63]	35	1.5
Water[a]	0	0
Sodium hydroxide pellets [64]	18	0.86
Sodium silicate (3.3WR, 37% solids) [65]	4.6	0.43

[a] Assumed negligible.

on CO_2 equivalent emissions from geopolymer and cement-concrete production conducted by Turner and Collins [51]. They assumed that liquid petroleum gas (LPG) was used for the temperature curing, and used a CO2-emission factor of 1.54 kg CO2-eq/L for LPG. To calculate the energy associated with the LPG use, the higher heating value (HHV) of 25.5 MJ/L [52] was used in this study.

For the reference studies, two types of cement concrete were considered: non-air-entrained (Non-AE) and air-entrained (AE) concrete, both of which were designed, based on the ACI 211 mix design method [53], to have 6000 psi (41 MPa) compressive strength (i.e. similar strength to the developed EGC materials). For ECC materials, the most studied version – M45 [54] – and a greener version that contains high volumes of fly ash (FA/C = 2.8) – HVFA ECC [55] – were examined. The mixture designs of those materials are shown in Table 13.

5.2. Results and discussion

Fig. 7 shows the computed energy- and carbon-MSI of the EGC, concrete, and ECC materials. As a result of optimizations during the matrix and composite design phases, the embodied energy of the preliminary EGC is reduced from 5.95 to 5.12 GJ/m^3 in EGC-1.5%, while the GWI from 325 to 291 kg CO_2-eq/m^3. Therefore, with the aid of the proposed integrate design method, 14 and 10% reduction

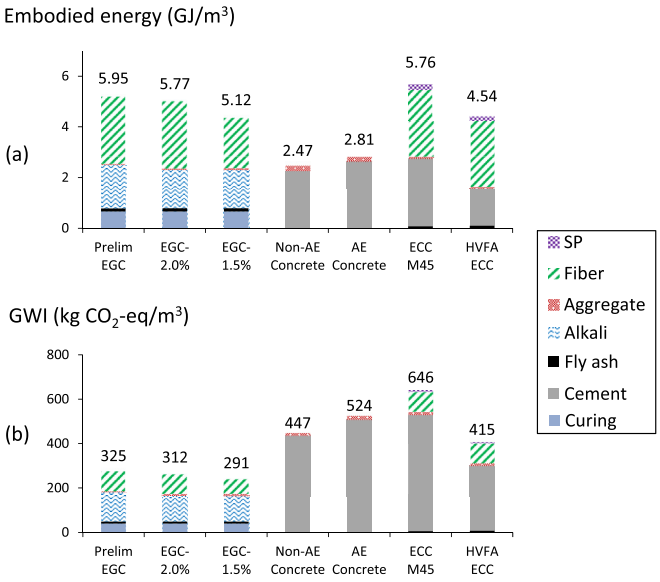

Fig. 7. (a) Embodied energy and (b) global warming intensity for EGC, concrete, and ECC materials.

was achieved in the embodied energy and carbon equivalent emissions, respectively.

The significant contributors in the embodied energy of EGC series are the alkaline activator and PVA fiber, which account for 40 and 46%, respectively, of the total energy for EGC-2.0% and 45 and 38% for EGC-1.5%. While the total energy consumption of EGC is greater than that of concrete, the geopolymer binder (i.e. energy associated with fly ash, alkaline activator, and temperature curing) consumes comparable energy to the cement binder in normal concrete. The use of the energy-intensive PVA fiber is responsible for the high energy consumption of EGC. The large embodied energy of the synthetic fiber is associated with the 'feedstock energy' (i.e. heat content of the petroleum-based ingredients), as well as the consumed energy for the manufacturing process. Due to the

Table 13
Mixture proportions of EGC, concrete, and ECC materials (in kg/m^3).

	Prelim EGC	EGC-2.0%	EGC-1.5%	Non-AE concrete[a]	AE concrete[a]	ECC M45	HVFA ECC
Type I cement				470	547	571	324
Coarse aggregate				1079	1079		
Fine aggregate				647	492		
Fine silica sand	340	460	463			456	456
Fly ash	1131	1151	1157			685	906
PVA fiber	26	26	19.5			26	26
SP						6.8	5.3
Water	179	142	142	193	175	332	320
NaOH (pellet)	63.5	59.8	60.1				
(pellets)							
Na_2SiO_3	289	259	260				

[a] Designed for compressive strength of 6000 psi (41 MPa), slump of 3 in (76 mm), maximum aggregate size of 1 in (25 mm), fine aggregate modulus of 2.80, and absorption capacity of 0.5% and 0.7% for coarse and fine aggregate, respectively. The air contents of Non-AE and AE concrete are 1% and 4.5%, respectively.

high energy intensity of the PVA fiber, ECC materials also have larger embodied energy than normal concrete. With the smaller fiber volume, EGC-1.5% has 11% less embodied energy than EGC-2.0%.

In the case of carbon equivalent emissions, EGC materials show an excellent performance; GWI of EGC-1.5% is 56–65% of those of concrete materials, and 30% less even when compared with the green HVFA ECC. Unlike the embodied energy, the carbon footprints of the PVA fiber are moderate, which offers an advantage in the GWI reduction. On the other hand, high GWI values of concrete and ECC are a result of the high carbon intensity of cement materials; indeed, production of 1 kg of Portland cement is estimated to emit 0.84–1.15 kg of CO_2 [56], contributing 5–8% to the global man-made CO_2 emissions [57] [58]. Therefore, use of no cement materials in EGC has a significant impact on the GWI reduction. In addition, by minimizing the fiber content, a further reduction in the carbon footprints is possible as demonstrated in EGC-1.5%.

6. Conclusion

This paper proposed a novel design methodology of Engineered Geopolymer Composite (EGC) that integrates the design of experiment (DOE), micromechanical modeling and life cycle analysis (LCA) methods. The integrated design method was applied to a preliminary version of EGC (with compressive strength of 27.6 MPa and tensile ductility of 4.3%) to achieve three design objectives simultaneously: to improve compressive strength, maintain high tensile ductility, and enhance the material greenness. As a result, an optimized EGC with compressive strength of 43.1 MPa and tensile ductility of 5.3% was successfully developed, while reducing 14% embodied energy and 10% CO_2 equivalent emissions compared with the preliminary EGC. The embodied energy and GWI of the optimized EGC are 11 and 55% lower, respectively, than a standard version of ECC (M45). The applicability and effectiveness of the proposed design method were demonstrated through the systematic design process and the achieved results.

In addition, the following new findings were obtained during the investigation;

- Compressive strength of EGC matrix increases when a larger amount of fly ash with higher calcium content – even those classified as class F (i.e. low-calcium) fly ash – is incorporated.
- EGC matrix has relatively low tensile strength and more brittle behavior compared with ECC matrix materials, while the compressive strength is comparable. This is, however, beneficial in achieving robust tensile strain-hardening and multiple cracking.
- Strong chemical bond, weak frictional bond and small slip-hardening coefficient were found in EGC, which contribute to smaller crack width and higher tensile ductility.
- The optimized EGC shows high tensile ductility of 3.0% even with the small fiber volume fraction of 1.0%. However, due to a small margin between the first cracking strength and fiber bridging capacity, variability among specimens is larger than EGC with higher fiber contents.
- EGC materials have a significant advantage in terms of the global warming intensity (GWI) associated with the material production. Although the embodied energy of EGC is higher than normal concrete, improvement is possible by reducing the volume fractions of energy-intensive PVA fiber.
- EGC with 1.5% PVA fiber shows balanced properties in tension and compression, and in MSI. This composite has suitable mechanical properties for civil infrastructure applications and support infrastructure sustainability through a low GWI.

The proposed design method is applicable to not only fly ash-based fiber-reinforced geopolymer but most other types of fiber-reinforced brittle matrix composites. The efficient and systematic design process facilitates the research and development of high performance sustainable construction composite materials.

Acknowledgements

This work was supported by the National Science Foundation (Grant CMMI 1068005 to the University of Michigan) and the support is gratefully acknowledged. The authors also acknowledge the material suppliers Headwaters Resources (Fly ash), PQ Corporation (Sodium silicate), and Kuraray (PVA fiber) for providing materials used in this study.

References

[1] A.R. Sakulich, Reinforced geopolymer composites for enhanced material greenness and durability, Sustain. Cities Soc. 1 (2011) 195–210, https://doi.org/10.1016/j.scs.2011.07.009.
[2] J. Davidovits, Geopolymer Chemistry and Applications, third ed., Institut Geopolymere, Saint-Quentin (France), 2008.
[3] P. Duxson, A. Fernández-Jiménez, J.L. Provis, G.C. Lukey, A. Palomo, J.S.J. Van Deventer, Geopolymer technology: the current state of the art, J. Mater. Sci. 42 (2007) 2917–2933, https://doi.org/10.1007/s10853-006-0637-z.
[4] J.L. Provis, J.S.J. van Deventer, Geopolymers-structure, Processing, Properties and Industrial Applications, Woodhead Publishing, Cambridge (UK), 2009.
[5] V.C. Li, On engineered cementitious composites (ECC). A review of the material and its applications, J. Adv. Concr. Technol. 1 (2003) 215–230, https://doi.org/10.3151/jact.1.215.
[6] M. Kunieda, K. Rokugo, Recent progress on HPFRCC in Japan required performance and applications, J. Adv. Concr. Technol. 4 (2006) 19–33, https://doi.org/10.3151/jact.4.19.
[7] J. Davidovits, Global warming impact on the cement and aggregates industries, World Resour. Rev. 6 (1994) 263–278.
[8] M. Weil, K. Dombrowski, A. Buchwald, Life-cycle analysis of geopolymers, in: J.L. Provis, J.S.J. van Deventer (Eds.), Geopolymers - Struct. Process. Prop. Ind. Appl, Woodhead Publishing, Cambridge (UK), 2009, pp. 194–210, https://doi.org/10.1533/9781845696382.2.194.
[9] B.C. McLellan, R.P. Williams, J. Lay, A. Van Riessen, G.D. Corder, Costs and carbon emissions for geopolymer pastes in comparison to ordinary portland cement, J. Clean. Prod. 19 (2011) 1080–1090, https://doi.org/10.1016/j.jclepro.2011.02.010.
[10] C. Ouellet-Plamondon, G. Habert, Life cycle assessment (LCA) of alkali-activated cements and concretes, in: F. Pacheco-Torgal, J. Labrincha, C. Leonelli, A. Palomo, P. Chindaprasit (Eds.), Handb. Alkali-activated Cem. Mortars Concr, Woodhead Publishing Limited, 2015, pp. 663–686, https://doi.org/10.1533/9781782422884.5.663.
[11] M. Şahmaran, V.C. Li, Durability properties of micro-cracked ECC containing high volumes fly ash, Cem. Concr. Res. 39 (2009) 1033–1043, https://doi.org/10.1016/j.cemconres.2009.07.009.
[12] M.D. Lepech, V.C. Li, Long term durability performance of engineered cementitious composites, Restor. Build. Monum. 2 (2006) 119–132.
[13] V.C. Li, Engineered cementitious composites (ECC) – material, structural, and durability performance, in: E.G. Nawy (Ed.), Concr. Constr. Eng. Handb, CRC Press, 2008, pp. 1–40.
[14] F.U.A. Shaikh, Deflection hardening behaviour of short fibre reinforced fly ash based geopolymer composites, Mater. Des. 50 (2013) 674–682, https://doi.org/10.1016/j.matdes.2013.03.063.
[15] M. Ohno, V.C. Li, A feasibility study of strain hardening fiber reinforced fly ash-based geopolymer composites, Constr. Build. Mater. 57 (2014) 163–168, https://doi.org/10.1016/j.conbuildmat.2014.02.005.
[16] B. Nematollahi, J. Sanjayan, F.U.A. Shaikh, Tensile strain hardening behavior of PVA fiber-reinforced engineered geopolymer composite, J. Mater. Civ. Eng. 27 (2015), https://doi.org/10.1061/(ASCE)MT.1943-5533.
[17] B. Nematollahi, J. Sanjayan, F.U.A. Shaikh, Comparative deflection hardening behavior of short fiber reinforced geopolymer composites, Constr. Build. Mater. 70 (2014) 54–64, https://doi.org/10.1016/j.conbuildmat.2014.07.085.
[18] G. Taguchi, System of Experimental Design: Engineering Methods to Optimise Quality and Minimize Cost, UNIPUB/Kraus International Publications, White Plains, New York, 1987.
[19] P.J. Ross, Taguchi Techniques for Quality Engineering: Loss Function, Orthogonal Experiments, Parameter and Tolerance Design, Second ed., McGraw Hill Professional, New York, NY, 1996.
[20] V.C. Li, Engineered cementitious composites (ECC) – tailored composites through micromechanical modeling, in: N. Banthia, A. Bentur, A.A. Mufti (Eds.), Fiber Reinf. Concr. Present Futur, Canadian Society for Civil Engineering, Montreal (Canada), 1998, pp. 64–97.
[21] G.A. Keoleian, A.M. Kendall, M.D. Lepech, V.C. Li, Guiding the design and application of new materials for enhancing sustainability performance:

framework and infrastructure application, Mater. Res. Soc. Symp. Proc. 895 (2006).
[22] ASTM C618, Standard Specification for Coal Fly Ash and Raw or Calcined Natural Pozzolona for Use in Concrete, ASTM International, West Conshohocken, PA, 2015. https://doi.org/10.1520/C0618-15.
[23] D. Hardjito, B.V. Rangan, Development and Properties of Low-calcium Fly Ash-based Geopolymer Concrete, Research report GC 1, Curtin University, Perth (Australia), 2005.
[24] J. Temuujin, A. van Riessen, R. Williams, Influence of calcium compounds on the mechanical properties of fly ash geopolymer pastes, J. Hazard Mater. 167 (2009) 82–88, https://doi.org/10.1016/j.jhazmat.2008.12.121.
[25] C.K. Yip, G.C. Lukey, J.S.J. Van Deventer, The coexistence of geopolymeric gel and calcium silicate hydrate at the early stage of alkaline activation, Cem. Concr. Res. 35 (2005) 1688–1697, https://doi.org/10.1016/j.cemconres.2004.10.042.
[26] R.N. Thakur, S. Ghosh, Effect of mix composition on compressive strength and microstructure of fly ash based geopolymer composites, J. Eng. Appl. Sci. 4 (2009) 68–74.
[27] A. Fernández-Jiménez, A. Palomo, Composition and microstructure of alkali activated fly ash binder: effect of the activator, Cem. Concr. Res. 35 (2005) 1984–1992, https://doi.org/10.1016/j.cemconres.2005.03.003.
[28] S. Thokchom, P. Ghosh, S. Ghosh, Effect of Na_2O content on durability of geopolymer mortars in sulphuric acid, J. Civil Environ. Struct. Constr. Archit. Eng. 3 (2009) 193–198.
[29] S. Thokchom, P. Ghosh, S. Ghosh, Effect of Na_2O content on durability of geopolymer pastes in magnesium sulfate solution, Can. J. Civ. Eng. 39 (2012) 34–43, https://doi.org/10.1139/l11-107.
[30] Y.K. Cho, S.W. Yoo, S.H. Jung, K.M. Lee, S.J. Kwon, Effect of Na_2O content, SiO_2/Na_2O molar ratio, and curing conditions on the compressive strength of FA-based geopolymer, Constr. Build. Mater. 145 (2017) 253–260, https://doi.org/10.1016/j.conbuildmat.2017.04.004.
[31] Z. Xie, Y. Xi, Hardening mechanisms of an alkaline-activated class F fly ash, Cem. Concr. Res. 31 (2001) 1245–1249, https://doi.org/10.1016/S0008-8846(01)00571-3.
[32] D. Marshall, B.N. Cox, A J-integral method for calculating steady-state matrix cracking stresses in composites, Mech. Mater. 7 (1988) 127–133.
[33] V.C. Li, C.K.Y. Leung, Steady-state and multiple cracking of short random fiber composites, J. Eng. Mech. 118 (1992) 2246–2264, https://doi.org/10.1061/(ASCE)0733-9399(1992)118:11(2246).
[34] A.A. Griffith, The phenomena of rupture and flow in solids, Philos. Trans. R. Soc. A Math. Phys. Eng. Sci. 221 (1921) 163–198, https://doi.org/10.1098/rsta.1921.0006.
[35] A. Katz, V.C. Li, A special technique for detemining the bond strength of carbon fibers in cement matrix by pullout test, J. Mater. Sci. Lett. 15 (1996) 1821–1823.
[36] C. Redon, V.C. Li, C. Wu, H. Hoshiro, T. Saito, A. Ogawa, Measuring and modifying interface properties of PVA fibers in ECC matrix, J. Mater. Civ. Eng. 13 (2001) 399–406, https://doi.org/10.1061/(ASCE)0899-1561(2001)13:6(399).
[37] V.C. Li, Y. Wang, S. Backer, A micromechanical model of tension-softening and bridging toughening of short random fiber reinforced brittle matrix composites, J. Mech. Phys. Solids 39 (1991) 607–625, https://doi.org/10.1016/0022-5096(91)90043-N.
[38] V.C. Li, C. Wu, S. Wang, A. Ogawa, T. Saito, Interface tailoring for strain-hardening polyvinyl alcohol-engineered cementitious composite (PVA-ECC), ACI Mater. J. 99 (2002) 463–472, https://doi.org/10.14359/12325.
[39] ASTM E399-12e3, Standard Test Method for Linear-elastic Plane-strain Fracture Toughness K1C of Metallic Material, ASTM International, West Conshohocken, PA, 2012, https://doi.org/10.1520/E0399-12E03.2.
[40] M. Li, V.C. Li, Cracking and healing of engineered cementitious composites under chloride environment, ACI Mater. J. 108 (2011) 333–340.
[41] B. Felekoglu, K. Tosun-Felekoglu, R. Ranade, Q. Zhang, V.C. Li, Influence of matrix flowability, fiber mixing procedure, and curing conditions on the mechanical performance of HTPP-ECC, Compos. Part B Eng. 60 (2014) 359–370, https://doi.org/10.1016/j.compositesb.2013.12.076.
[42] E.-H. Yang, S. Wang, Y. Yang, V.C. Li, Fiber-bridging constitutive law of engineered cementitious composites, J. Adv. Concr. Technol. 6 (2008) 181–193, https://doi.org/10.3151/jact.6.181.
[43] T. Kanda, V.C. Li, Interface property and apparent strength of high-strength hydrophilic fiber in cement matrix, J. Mater. Civ. Eng. 10 (1998) 5–13, https://doi.org/10.1061/(ASCE)0899-1561(1998)10:1(5).
[44] J. Morton, G.W. Groves, The effect of metal wires on the fracture of a brittle-matrix composite, J. Mater. Sci. 11 (1976) 617–622, https://doi.org/10.1007/BF01209446.
[45] V.C. Li, Postcrack scaling relations for fiber reinforced cementitious composites, J. Mater. Civ. Eng. 4 (1992) 41–57, https://doi.org/10.1061/(ASCE)0899-1561(1992)4:1(41).
[46] S. Wang, V.C. Li, High-early-strength engineered cementitious composites, ACI Mater. J. 103 (2006) 97–105.
[47] E. Yang, Designing Added Functions in Engineered Cementitious Composites, University of Michigan, Ann Arbor, 2008.
[48] T. Kanda, V.C. Li, Practical design criteria for saturated pseudo strain hardening behavior in ECC, J. Adv. Concr. Technol. 4 (2006) 59–72, https://doi.org/10.3151/jact.4.59.
[49] E. Yang, V. Li, Numerical study on steady-state cracking of composites, Compos. Sci. Technol. 67 (2007) 151–156, https://doi.org/10.1016/j.compscitech.2006.07.012.
[50] G. Myhre, D. Shindell, F. Bréon, W. Collins, J. Fuglestvedt, J. Huang, D. Koch, J. Lamarque, D. Lee, B. Mendoza, T. Nakajima, A. Robock, G. Stephens, T. Takemura, H. Zhang, Anthropogenic and natural radiative forcing, in: T.F. Stocker, D. Qin, G.-K. Plattner, M. Tignor, S.K. Allen, J. Boschung, A. Nauels, Y. Xia, V. Bex, P.M. Midgley (Eds.), Clim. Chang. 2013 Phys. Sci. Basis, Work. Gr. I Contrib. to Fifth Assess. Rep. Intergov. Panel Clim. Chang, Cambridge University Press, Cambridge (UK), 2013, p. 714, https://doi.org/10.17/CBO9781107415324.018.
[51] L.K. Turner, F.G. Collins, Carbon dioxide equivalent (CO_2-e) emissions: a comparison between geopolymer and OPC cement concrete, Constr. Build. Mater. 43 (2013) 125–130, https://doi.org/10.1016/j.conbuildmat.2013.01.023.
[52] US Eenvironmental Protectiion Agency, Direct Emissions from Mobile Combustion Sources, 2016. https://www.epa.gov/sites/production/files/2016-03/documents/mobileemissions_3_2016.pdf.
[53] ACI 211, Standard Practice for Selecting Proportions for Normal Heavyweight, and Mass Concrete (Reapproved 2009), American Concrete Institute, Farmington Hills, MI, 2009.
[54] S. Wang, Micromechanics Based Matrix Design for Engineered Cementitious Composites, University of Michigan, Ann Arbor, 2005.
[55] E.H. Yang, Y. Yang, V.C. Li, Use of high volumes of fly ash to improve ECC mechanical properties and material greenness, ACI Mater. J. 104 (2007) 620–628.
[56] J.S. Damtoft, J. Lukasik, D. Herfort, D. Sorrentino, E.M. Gartner, Sustainable development and climate change initiatives, Cem. Concr. Res. 38 (2008) 115–127, https://doi.org/10.1016/j.cemconres.2007.09.008.
[57] E. Worrell, L. Price, N. Martin, C. Hendriks, L. Ozawa Meida, Carbon dioxide emissions from the global cement industry, Annu. Rev. Energy Environ. 26 (2001) 303–329.
[58] P. Duxson, J. Provis, Low CO_2 concrete: are we making any progress?, in: BEDP Environ. Des. Guid, Australian Institute of Architects, Melbourne, Australia, 2008.
[59] M.L. Marceau, M.A. Nisbet, M.G. Vangeem, Life Cycle Inventory of Portland Cement Manufacture, Portland Cement Association, Stokie, IL, 2006.
[60] M.A. Nisbet, M.L. Marceau, M.G. Vangeem, Environmental Life Cycle Inventory of Portland Cement Concrete, Portland Cement Association, Stokie, IL, 2002.
[61] R. Ranade, Advanced Cementitious Composite Development for Resilient and Sustainable Infrastructure, University of Michigan, Ann Arbor, 2014.
[62] R. Frazão, R. Fernandes, Comparative Analysis of the Life Cycle of AT Fibre-cement and NT Fibre-cement, International Chrysotile Association, 2004.
[63] G.A. Keoleian, A. Kendall, J.E. Dettling, V.M. Smith, R.F. Chandler, M.D. Lepech, V.C. Li, Life cycle modeling of concrete bridge design: comparison of engineered cementitious composite link slabs and conventional steel expansion joints, J. Infrastruct. Syst. 11 (2005) 51–60, https://doi.org/10.1061/(ASCE)1076-0342(2005)11:1(51).
[64] E. Chlor, An Eco-profile and Environmental Product Declaration of the European Chlor-alkali Industry, 2013. https://www1.ethz.ch/ifu/ESD/education/master/AESEA/Euro_Chlor_Eco-profile_Chlorine_2014-03.pdf. (Accessed 10 March 2017).
[65] M. Fawer, M. Concannon, W. Rieber, Life cycle inventories for the production of sodium silicates, Int. J. Life Cycle Assess. 4 (1999) 207–212, https://doi.org/10.1007/BF02979498.